Manipulating Quantum Interference Effect and Magnetotransport of ZnO Nanowires through Interfacial Doping

Siwen Zhao,[abc] Yiming Wu,[abc] Kaixuan Zhang,[abc] Huaiyi Ding,[abc] Dongxue Du,[a] Jiyin Zhao,[a] Nan Pan*[abc] and Xiaoping Wang*[abc]

a. *Hefei National Laboratory for Physical Sciences at the Microscale, University of Science and Technology of China, Hefei, Anhui, P.R. China.*
E-mail: npan@ustc.edu.cn; xpwang@ustc.edu.cn
b. *Synergetic Innovation Center of Quantum Information & Quantum Physics, University of Science and Technology of China, Hefei, Anhui 230026, P. R. China.*
c. *Key Laboratory of Strongly-Coupled Quantum Matter Physics, Chinese Academy of Sciences, School of Physical Sciences, University of Science and Technology of China, Hefei, Anhui 230026, P. R. China.*

Supporting information

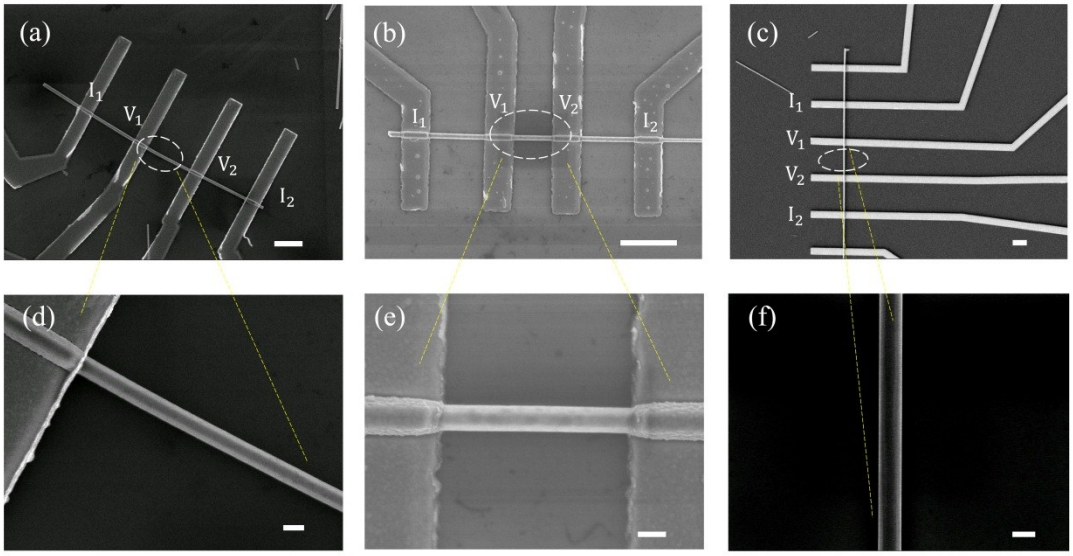

Figure S1 Scanning electron microscope (SEM) images of the (a) sample A, (b) sample B and (c) sample C devices. (d) to (f) are the magnified images of the marked regions in (a) to (c) in order to observe the diameters of the devices more clearly. Scale bars: 2μm in (a) to (c) and 200nm in (d) to (f).

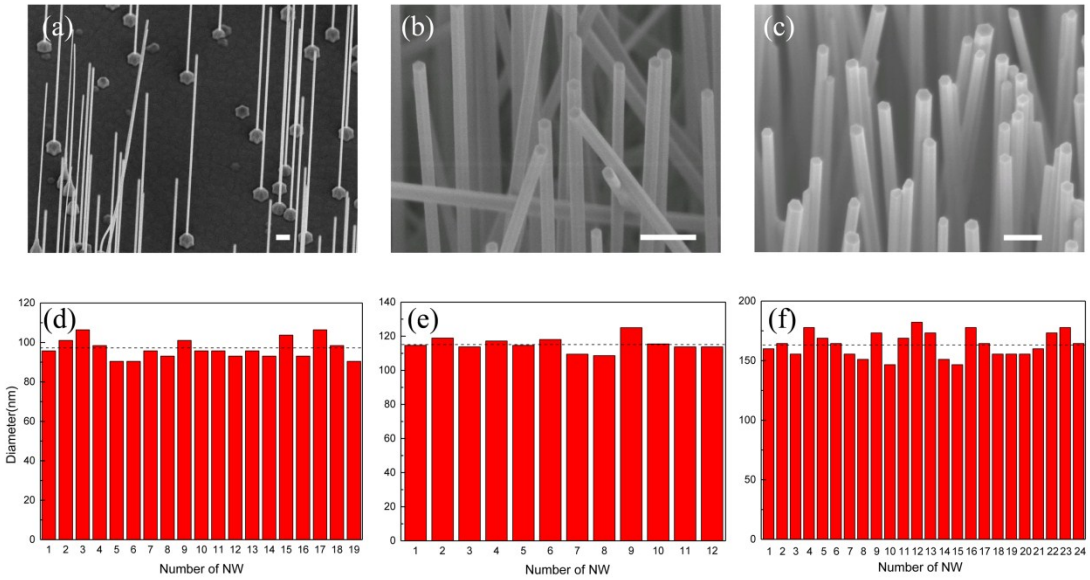

Figure S2 (a) to (c): SEM images of the core ZnO NWs for sample A, B and C. The scale bar in (a) to (c) are 500nm. (d) to (f): Statistical analysis of diameters of the NWs in (a) to (c).The dash lines in (d) to (f) represent the corresponding average diameters, which are 96.7nm, 115.3nm and 163.5nm, respectively. Note that the average diameter of core NWs is not the central diameter of the doping channel D_i. As shown in the schematic illustration in Fig. 1(b) in the manuscript, D_i is equal to the sum of the thickness of interfacial doping channel W_i and the average diameter of core ZnO NWs.

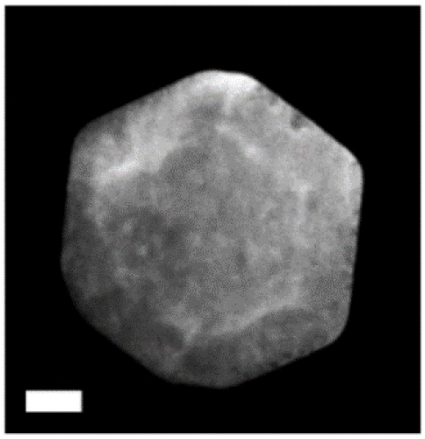

Figure S3 HAADF STEM image of the IND NW (sample A). Scale bar: 20 nm.

In the following, we briefly describe how to obtain the data in Table 1 in the main text.

Taking sample A as an example, the average and error estimate of the overall diameter of NW *d*, and the length between the two voltage leads *L* are obtained by repeated measuring the SEM

image of sample A for twenty times carefully. The same process is applied for sample B and sample C.

Because it is impossible to *in-situ* get the thickness of interfacial doping channel W_i of the devices without destroying the device, we adopt an alternative method. We used the same batch of samples for making devices as well as characterizing the cross section by STEM (such as Fig1(b) and Fig.S3). Since the growth procedure and conditions were completely the same, W_i of each device essentially has no difference with the corresponding sample for the cross-sectional STEM characterization. Therefore, we can obtain the values of W_i for samples A, B and C, as summarized in Table R1, from the representative STEM images with the same statistical method mentioned above.

As shown in the schematic illustration in Fig. 1(b) in the main text, the central diameter of the doping channel D_i is equal to the sum of W_i and the average diameter of core ZnO NWs. Through the statistical analysis of NWs in Figs. S2(a) to (c), the average diameters of the core NWs for sample A, B and C can be obtained in Figs. S2(d) to (f). By adding the W_i together with the average diameters of the core NWs, D_i and its error estimate can be derived.

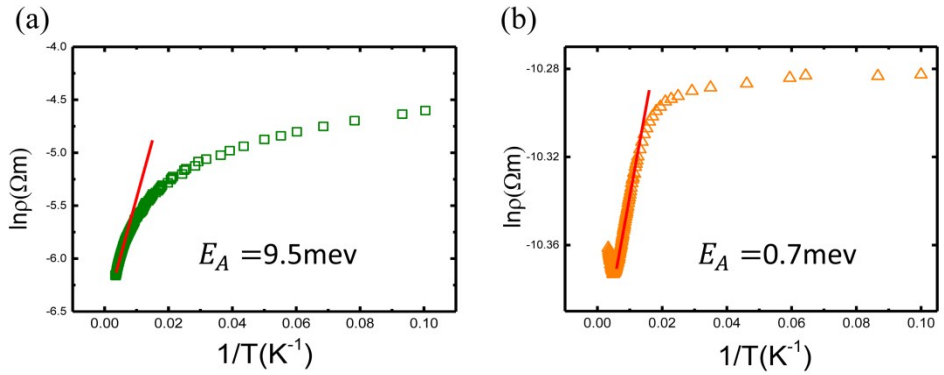

Figure S4 The Arrhenius fitting to determine the activation energy of (a) sample A and (b) sample B.

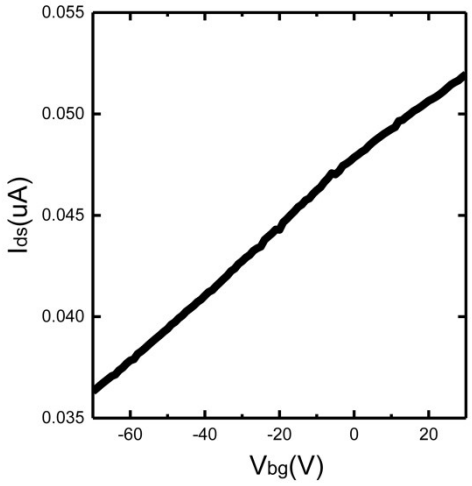

Figure S5 The transfer characteristics of the sample A at 10K.

The average concentration of the carriers in the IND ZnO NW can be deduced from the transfer characteristics of FET as shown in Figure S3. However, the gate modulation is unavailable in the IAD ZnO NWs FET because of the high doping. Therefore, the carrier concentration in the IAD ZnO NWs is estimated as below.

The thickness of AlOx deposited by ALD is about 0.2nm. STEM characterization reveals that the thickness of the interfacial doping region is about 7nm. Assumed that x=3/2, the concentration of the dopants can be calculated to be about:

$$N = \frac{\rho V_{AlOx}}{M_{AlOx} V_{interface}} \approx 8 \times 10^{20}/cm^3$$

For sample B, the activation energy is about $0.7mev$. Therefore, the average concentration of the carriers is about $5.1 \times 10^{19}/cm^3$. For sample C, the dopants are totally ionized, leading the average carrier concentration to be about $1.3 \times 10^{20}/cm^3$.

Moreover, based on the free electron model, we also calculated the Fermi wavenumber k_F, the mean free path l and the diffusion coefficient D for all samples, and the results at 10 K are demonstrated in Table S1.

Table S1. Sample parameters at 10K. *D* is the electron diffusion constant, *l* is the electron elastic mean-free path, and k_F is the Fermi wave number.

	$n(\mathrm{cm}^{-3})$	$D(\mathrm{cm}^2\mathrm{s}^{-1})$	$l(\mathrm{nm})$	$k_F(\mathrm{nm}^{-1})$	$k_F l$
sample A	9×10^{18}	0.03	0.03	0.6	0.02
sample B	5.1×10^{19}	4.3	2.6	1.1	2.9
sample C	1.3×10^{20}	10.0	4.7	1.6	7.4

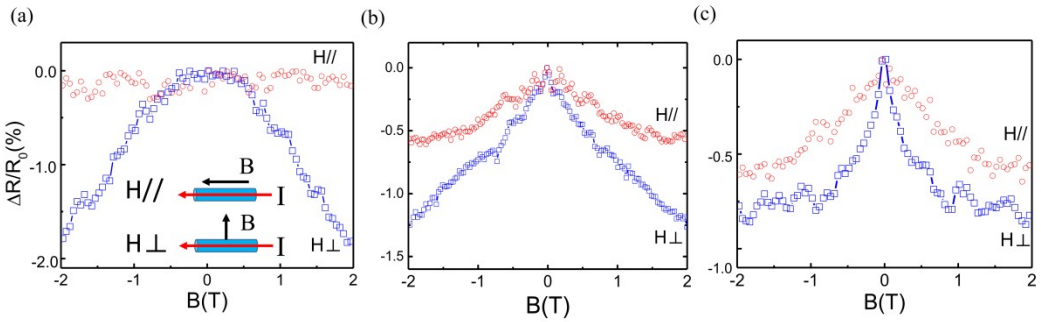

Figure S6 Comparison of the parallel (red) and perpendicular (blue) normalized MR of (a) sample A, (b) sample B and (c) sample C at 2K. The inset in (a) shows the illustration of measurement.

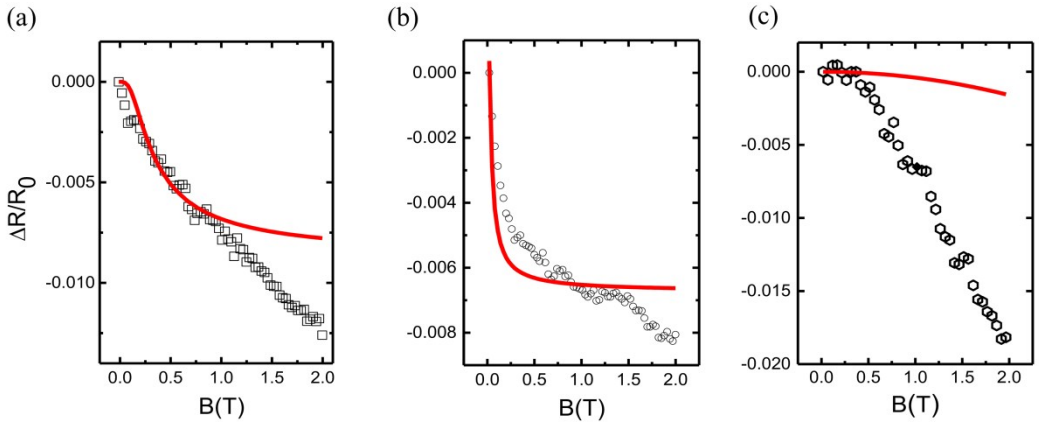

Figure S7 Low-field perpendicular normalized MR of (a) sample A (b) sample B and (c) sample C at 2K. The solid lines are the fits according to the 1D weak localization theory.

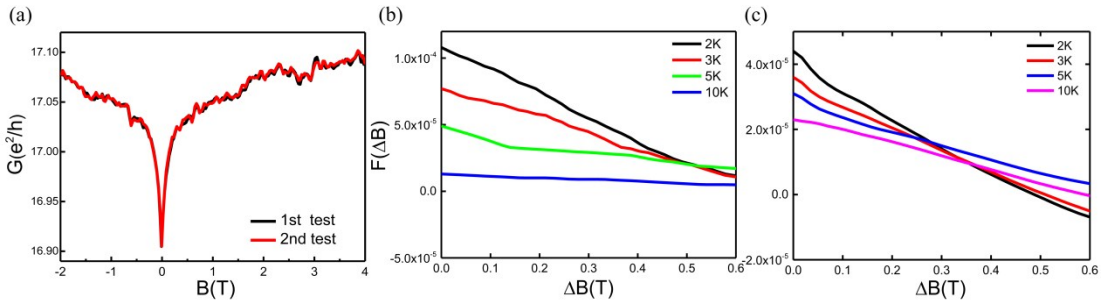

Figure S8 (a) Two magneto-conductance traces measured at 2K (black and red curves) indicative of excellent reproducibility of the conductance fluctuations in sample C. Autocorrelation functions F(ΔB) of the magneto-conductance traces at different temperatures for (b) sample B and (c) sample C.

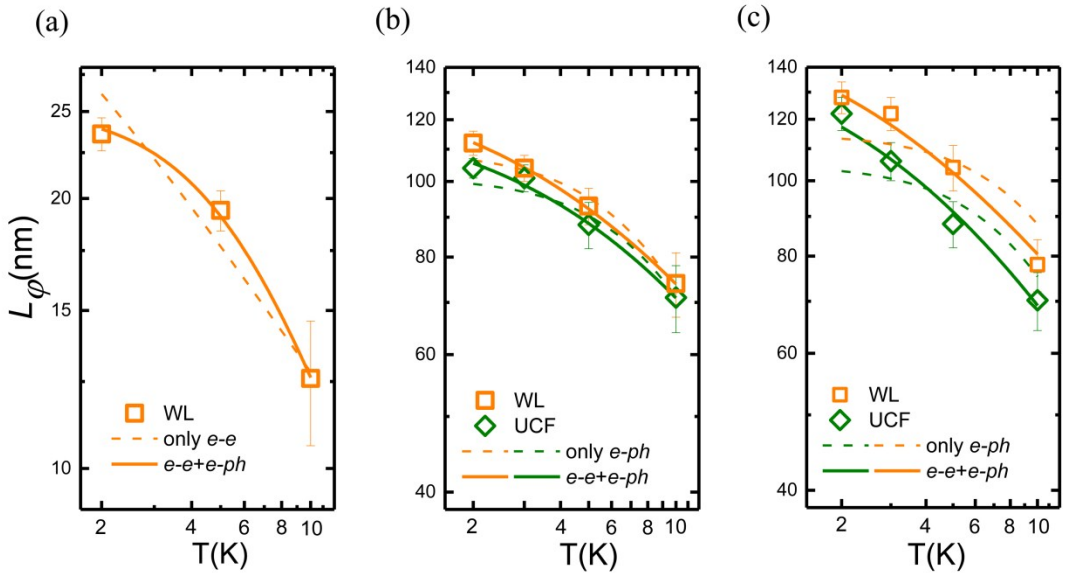

Figure S9 Temperature dependence of phase-coherent length L_φ in (a) sample A, (b) sample B and (c) sample C. The solid curves show the fits of the data according to the Eq. 2. The dashed line in (a) is the fit considering only *e-e* interaction and the dashed lines in (b) and (c) are the fits considering only *e-ph* interaction.

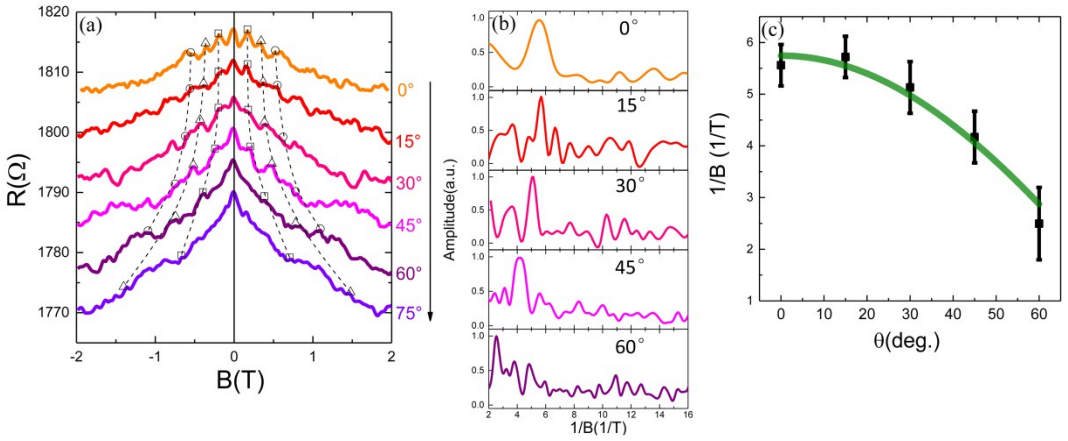

Figure S10 (a) AAS periodic oscillations at different tilting angles from 0° to 75° with B as the horizontal ordinate for sample B at 2K. (b) The corresponding FFT for sample B at different tilting angle. (c) The angle dependence of 1/B. The green line is the fitting result using the function $1/B = cos\theta/B_0$